AIAA JOURNAL
Vol. 49, No. 1, January 2011

Experimental and Numerical Investigation of Flow Properties of Supersonic Helium–Air Jets

Steven A. E. Miller*
NASA Langley Research Center, Hampton, Virginia 23681
and
Jérémy Veltin†
Pennsylvania State University, University Park, Pennsylvania 16802

DOI: 10.2514/1.J050720

Heated high-speed subsonic and supersonic jets operating on- or off-design are a source of noise that is not yet fully understood. Helium–air mixtures can be used to simulate the total temperature ratio of heated jets and hence have the potential to provide inexpensive and reliable flow and acoustic measurements. Accurate knowledge of the mean flow is a crucial initial step for a complete understanding of the noise generation mechanisms. This study focuses on providing close comparisons between measured mean flow properties of helium–air mixture jets and results from simulations of similar mixed jets as well as heated air jets. Axisymmetric supersonic jets issuing from convergent and convergent-divergent nozzles are investigated, and the results show good agreement with heated air jet measurements. The flow properties are examined in detail to demonstrate the validity of simulating heat with the addition of helium. Excellent agreement is obtained in the presented data between the numerical predictions and the experiments, further justifying the helium addition methodology, as well as validating the frozen chemistry model used in the numerical simulations.

Nomenclature

a	=	speed of sound
c	=	specific heat
D	=	nozzle exit diameter
H	=	enthalpy
M	=	Mach number
M_d	=	nozzle design Mach number
M_∞	=	acoustic Mach number (U_j/a_∞)
P	=	pressure
P_p	=	pitot pressure
R	=	gas constant
r	=	radial direction, coordinate
S	=	entropy
T	=	temperature
U	=	mean velocity
x	=	downstream direction, coordinate

Greek

γ	=	ratio of specific heats
δ_ω	=	the vorticity thickness
η	=	normalized radial distance
ρ	=	density
Φ	=	mass fraction
χ	=	molar fraction

Subscripts

j	=	jet exit fully-expanded quantity
t	=	total or stagnation quantity
1	=	local quantity
2	=	quantity measured behind the shock created by the pitot probe
∞	=	atmospheric quantity

Superscript

air	=	quantity relating to air
He	=	quantity relating to helium
heated	=	quantity relating to heated air
mix	=	quantity relating to a helium–air mixture

Introduction

MILITARY aircraft jet engines have noise characteristics much louder than civilian aircraft due to their very low bypass ratio, high exhaust temperature, and high exhaust velocities. The high intensity noise generated by these heated subsonic or supersonic jets is a health hazard to ground crews as well as an annoyance to communities in the vicinity of airfields. This has led to a need for reduction of jet noise by developing noise suppression mechanisms that include new nozzle design concepts such as chevrons, corrugations, beveled nozzles, or other nonaxisymmetric geometries. Research by Tanna et al. [1], Lau [2], Seiner et al. [3], and Tam and Chen [4] demonstrated that there are significant differences in how moderately heated supersonic jets generate noise compared with their unheated counterparts. Mixing noise is present in all jets and is caused by the coherent and incoherent turbulent structures. Adding some heating to a supersonic air jet helps to stabilize the instability waves in the shear layer, but when these instability waves travel faster than the ambient speed of sound, Mach wave radiation occurs in addition to the mixing noise. Jets operating supersonically and off-design also exhibit shock noise which is dominant in the upstream direction.

To study jets under realistic engine operating conditions, heating is required so that the convection velocity of the turbulent structures is supersonic and the effects of Mach wave radiation can be measured. In practical terms, a heated jet facility involves significant complexity and expense. To avoid this, the low density and high velocity of hot jets have been simulated in previous studies [5–7] by using a gas of

Presented as Paper 2010-471 at the 48th AIAA Aerospace Sciences Meeting Including the New Horizons Forum and Aerospace Exposition, Orlando, FL, 4–7 January 2010; received 14 June 2010; revision received 28 September 2010; accepted for publication 30 September 2010.

*Research Aerospace Engineer, Aeroacoustics Branch, 2 North Dryden Street, Mail Stop 461; s.miller@nasa.gov. Member AIAA.

†Postdoctoral Researcher, Aerospace Engineering Department.

lower density than air, like helium. By using a helium–air mixture, it becomes possible to simulate either the density or the acoustic velocity of a heated jet without having to heat the air. Although there are some differences between an actual heated jet and the preceding described simulated experiment, the major features of the noise generation process seem well represented and lead to satisfactory results in previous studies [5–7]. However, as noise reduction concepts are being investigated, with increasing demand on the accuracy of the acoustic and flow measurements, a detailed assessment of the limits of the simulation of hot air jets with helium–air mixtures needs to be made. The present study investigates the details of the mean flow properties of both heated and heat-simulated jets, using a combination of experimental measurements and computational fluid dynamics (CFD) simulations. Experiments performed with cold, pure air jets and with helium–air mixtures highlight the effects of simulated heat on the jet flow properties. Numerical results with cold and heated pure air jets as well as helium–air mixture jets are used to assess the validity of the helium addition to properly simulate heating.

Approach

The purpose of this study is to provide detailed comparisons between the mean flow properties of helium–air mixture jets with heated jets. A short description of the simulation of heated jets with a helium–air mixture is presented. Then the experimental and computational approaches are described.

Simulating Heating with Helium–Air Mixtures

The temperature of the jet flow has substantial effects on the resultant noise. A heated jet has different physical characteristics than a cold jet, due to the increase in jet exit velocity and decrease in jet density. To make acoustic measurements of a heated jet, considerable cost and safety issues are a concern in laboratory facilities. An alternative to heating the jet is to create a jet flow that is unheated but has similar properties that correspond to a heated jet. This avoids the power, infrastructure, and operating cost requirements of a heated jet facility [8]. This is accomplished by mixing helium with air. Helium was chosen for its low density, high acoustic velocity, and the fact that it is an inert gas that is inexpensive to obtain and handle. This methodology was developed at the Pennsylvania State University by Kinzie and McLaughlin [6] and Doty and McLaughlin [5]. A similar methodology is being used by Papamoschou [7] at the University of California Irvine. For acoustic measurements the quantities that need to be matched between a helium–air and heated jet are the ratio of acoustic velocities a_j/a_∞ and the ratio of jet densities ρ_j/ρ_∞. Matching both of these quantities will ensure that the fully-expanded Mach numbers and other nozzle exit properties of both jets are the same. A consequence is that the nozzle pressure ratio between the two conditions is slightly different due to variations of the ratios of specific heat γ between air and a helium–air mixture.

An experiment can be conducted to match both quantities if helium is mixed with the ambient air in the anechoic chamber as mentioned by Kinzie and McLaughlin [6], however, this approach is impractical. One needs to choose whether to perform an experiment matching the density or acoustic velocity if the ambient exhaust medium can not be modified. In prior experimental work by Doty and McLaughlin [5], the two parameter matching methods were investigated, with direct comparisons to heated air measurements. Only very small variations in the acoustic spectrum were observed and were of the same order of magnitude as the experimental uncertainty of the measurements. More recent careful comparisons [9] with measurements performed in other facilities have shown very good agreement when matching the acoustic velocity of the helium–air jet to that of a heated jet. Therefore, matching of the acoustic velocity is chosen for the experimental and numerical results presented in this study, meaning the mixture properties are defined such that

$$\left(\frac{a_j}{a_\infty}\right)^{\text{heated}} = \left(\frac{a_j}{a_\infty}\right)^{\text{mix}} \Leftrightarrow \sqrt{\gamma R T_j} = \sqrt{\gamma^{\text{mix}} R^{\text{mix}} T_j^{\text{mix}}} \quad (1)$$

Experimental Approach

Experimental measurements of the mean flow properties are performed using pitot probes within the jet plume. The schematic diagram presented in Fig. 1a shows the nomenclature used for the flow quantities around a single probe. The subscript $(\,)_2$ indicates the properties just downstream of the normal shock portion of the shock wave, immediately upstream of the pitot probe, and the subscript $(\,)_1$ indicates the local properties ahead of the shock. Figures 1b and 1c show photographs of the pitot probes used for the measurements. It consists of a rake of five probes of outer diameter 0.6 mm (0.025 in.) and inner diameter 0.25 mm (0.01 in.). Apart from this new probe rake, the overall experimental setup is the same as the one described in Miller et al. [10].

The pitot pressure P_p, can be used to find a value for the local Mach number M_1. Wherever the flow is supersonic, a shock forms in front of the probe, and P_p is equal to the total pressure behind the shock, P_{t2}. M_1 is then calculated using the Rayleigh pitot formula shown in Eq. (2). Wherever the flow is subsonic, there is no shock ahead of the probe, thus P_p is equal to P_{t1} and the isentropic flow formula of Eq. (3) can be used. Since the jets evaluated in this study are fully-expanded, the static pressure P_1 can be assumed to be constant and equal to the ambient static pressure P_∞ everywhere within the jet. A more detailed description of this processing is presented in Miller et al. [10] as well as some detailed comparisons between simulations and experimental measurements for pure (and unheated) air jets:

$$\frac{P_p}{P_1} = \left[\frac{(\gamma+1)M_1^2}{(\gamma-1)M_1^2+2}\right]^{\frac{\gamma}{\gamma-1}} \left[\frac{\gamma+1}{2\gamma M_1^2-(\gamma-1)}\right]^{\frac{1}{\gamma-1}} \quad (2)$$

$$\frac{P_p}{P_1} = \left[1+\frac{(\gamma-1)}{2}M_1^2\right]^{\frac{\gamma}{\gamma-1}} \quad (3)$$

Attempting to perform this calculation in a helium–air mixture jet leads to a complication: the mass concentration of helium Φ_1^{He} is not constant within the mixing layer, leading to fluctuations of properties such as the local specific heat ratio γ_1 across the jet. Since no measurement of the species concentration is available within such high-speed jets, an analytical approach needs to be used in order to yield estimates of the gas constitution. This approach detailed in the Appendix, leads to the conclusion that the mass concentration of helium varies in direct proportion with the local velocity.

The processing of the experimental data is performed with MATLAB. The pitot pressure P_p is used for producing an estimate of the local Mach number M_1 by using γ_j and T_j everywhere within the jet. Equation (2) (Rayleigh pitot formula) is first used for that purpose. In the regions where subsonic conditions exist, Eq. (3)

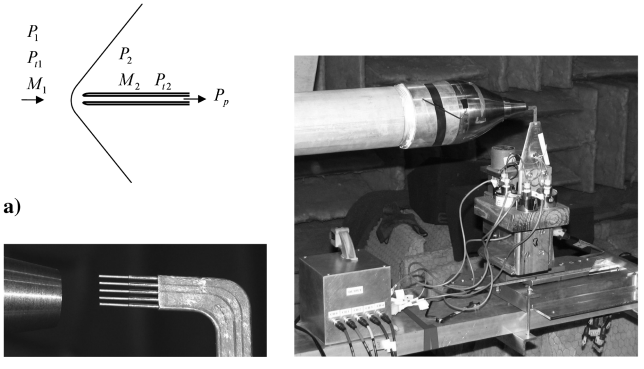

Fig. 1 The experimental setup showing a) schematic diagram of a pitot pressure probe in a freestream flow, b) detailed view of the pitot rake at the exit plane of a round nozzle, and c) pitot setup.

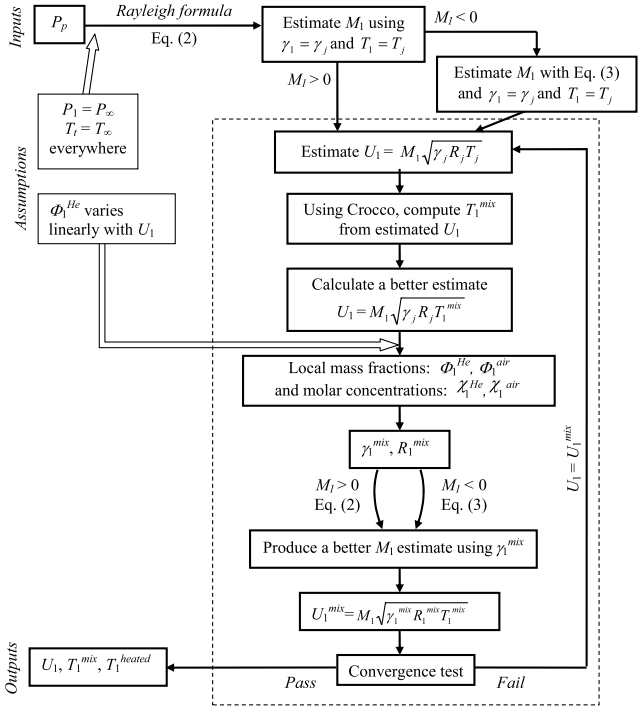

Fig. 2 Flowchart of the pitot measurement processing.

(isentropic flow formula) is used instead for a better estimate of M_1. Next an approximation of the local velocity is obtained, and from it the local static temperature, T_1 is computed using the Crocco relation. A better estimate of the velocity is then computed using the refined T_1. Then the mass and molar concentration of the species are evaluated, leading to an estimate for the local specific heat ratio and gas constant of the mixture. A refined velocity is computed from these values and the process is repeated until it converges to the final values for the local velocity U_1 and temperature T_1. Any other local property of the flow can be computed from these. The overall processing methodology is summarized in the flow chart of Fig. 2.

Computational Approach

In the previous section the experimental method and approach to find field-variables from helium–air jets is described. A numerical approach to find the same field-variables at the same spatial locations is discussed here. This numerical approach uses the Reynolds-averaged Navier–Stokes (RANS) equations, which are numerically integrated until a steady solution is achieved with the NPARC Alliance Wind-US 2.0 solver. Wind-US was developed by the NPARC Alliance which is a partnership between NASA Glenn Research Center and the U.S. Air Force Arnold Engineering Development Center, and additional contributors. A large number of validation cases of a broad range of flow-regimes have been made with the Wind-US solver by the NPARC Alliance. Wind-US can solve the Euler or Navier–Stokes equations in conjunction with many different turbulence models on structured or unstructured multiblock domains. It also has the ability to perform the computations in serial or parallel using the message passing interface or the parallel virtual machine. The Menter [11] shear stress transport (SST) turbulence model is used in the present simulations for both heated air and helium–air mixtures to close the steady RANS equations. In addition, transport equations are solved for each species of the flow. In this case a helium, oxygen, and nitrogen mixture is chosen to represent the helium–air mixture. The traditional ideal gas model is also used for corresponding heated air simulations with a constant γ. The turbulent Prandtl number is set in all simulations at 0.90 and Sc_t is set as 0.70.

Generally CFD simulations of jets use ideal gas such as air because corresponding laboratory measurements use unheated or heated air. Often CFD simulations assume that the gas constant and ratio of specific heats are constant. Unfortunately, this assumption does not allow for the variation of the thermodynamic quantities inside and outside the nozzle, where they differ because of the large temperature differences. In aircraft jet engines the combustion process adds additional species to air, also changing the thermodynamic quantities. Simulation of these combustion reactions is computationally expensive. In conventional aircraft engines the majority of the combustion process is complete when the gas reaches the nozzle inlet, therefore, a frozen chemistry model can be used. The assumption can also be made, as discussed in the Appendix, that diffusion is the only mechanism that changes the species concentration. Similar assumptions were made by Yoder et al. [12] with comparisons between the effects of using a ideal gas (air), ideal gas mixtures, and a frozen exhaust gas mixture for subsonic and supersonic jets.

In a helium–air mixture jet there is no combustion process and the number of species is relatively small compared with those produced in an aircraft engine. Since the helium–air mixture properties are known in the experiments and the only mixing occurs upstream of the nozzle, the mass species concentration is well known at the nozzle outlet. Far outside of the jet, the gas mixture corresponds to ambient air. Since no chemical process occurs in the shear layer of the jet, and mixing is mainly produced by turbulence, a frozen chemistry model is used in Wind-US.

Wind-US has the ability to perform reacting flow calculations with a preexisting chemistry model that is initialized with the addition of a keyword in the Wind-US input file. Frozen chemistry modeling is used for the helium–air simulations presented in this study, but not for the heated air simulations. Additional inputs required by the chemistry module consist of the species concentration in the far-field and at the inflow boundary at the nozzle inlet. The full implementation of the frozen chemistry module and associated transport equations without reaction sources can be found in the Wind-US documentation [13] or the Wind-US developer's reference.

Wind-US has a number of standard chemistry packages that contain various models of standard molecules. Unfortunately, none of these packages contain information for the element helium. An external chemistry file, developed by Joo Kyung Suh of the Raytheon Corporation, contains the species helium along with the two most abundant elements in air, oxygen and nitrogen. The chemistry file contains the thermodynamic coefficients of the three species, derived from McBride et al. [14] where three curves are defined for each species. These curves describe the specific heat at constant pressure, enthalpy, and entropy over a given range of temperatures in terms of coefficients a_i and b_i. The range of temperature for the three curves is from 200 to 20,000 K. Thermodynamic values defined by McBride et al. [14] based on the coefficients in the helium–air chemistry file are

$$c_p/R = a_1T^{-2} + a_2T^{-1} + a_3 + a_4T + a_5T^2 + a_6T^3 + a_7T^4 + a_8T^5 \tag{4}$$

$$H/(RT) = -a_1T^{-2} + a_2T^{-1}\ln T + a_3 + a_4T/2 + a_5T^2/3 + a_6T^3/4 + a_7T^4/5 + a_8T^5/6 + b_1/T \tag{5}$$

$$S/R = b_2 - a_1T^{-2}/2 - a_2T^{-1} + a_3\ln T + a_4T + a_5T^2/2 + a_6T^3/3 + a_7T^4/4 + a_8T^5/5 \tag{6}$$

where c_p is the specific heat at constant pressure, H is the enthalpy, R is the universal gas constant, S is the entropy, and T is the temperature. The chemistry file also contains the reaction rate coefficients for the three species with which Wind-US calculates the forward and backward reaction rates if necessary. Since only a three species model is available, other species that are typically present in small quantity in air, such as argon, are ignored. A similar assumption was made successfully by Yoder et al. [12]. The frozen chemistry model of a helium–air mixture has not been tested on high-speed subsonic or supersonic on- or off-design jets before. These

simulations represent the first steady helium–air mixture jet simulations for this flow regime that the authors are aware of.

Axisymmetric simulations are conducted, using computational grids developed to match the geometry of the nozzles used for the experiments, as described in more details in a previous study [10]. The axisymmetric form of the governing equations are solved. Two computational grids are used for this study. The first is for the converging nozzle, $M_d = 1.0$ and the second is for the converging-diverging nozzle, $M_d = 1.5$. The computational domain extends 75 D from the nozzle exit in the downstream direction, 50 D from the nozzle exit in the radial direction, and 5 D upstream from the nozzle inlet. Initial iterations are performed using a constant Courant–Friedrichs–Lewy number of 0.50 and then explicit Euler time stepping using a constant time step is used until the L^2 residual remains constant and a visual inspection of the solution appears steady. The L^2 residual is a global measure of the residual error of the governing equations of the flowfield. Grid independence studies are performed by using every other grid point in the computational domain in both the streamwise and radial directions. No difference in the steady solution between the sequenced (every other grid point used) and unsequenced grid is apparent in any of the solutions. The boundary layer at the nozzle exit is fully resolved by setting the first grid point in the viscous sublayer region using $y^+ = 1$, where y^+ is the coordinate of the viscous wall layer using average conditions [15].

Boundary conditions for the simulations consist of a downstream outflow in the streamwise direction allowing the flow to exit the computational domain. This assumes that the outflow is subsonic and the free-field pressure is set as the ambient pressure. Freestream boundary conditions are specified in the free-field where a small uniform flow at $M_\infty = 0.001$ is assumed for stability and the total ambient pressure is equal to the downstream static pressure. A standard axisymmetric boundary condition, which is essentially an inviscid wall, lies on the centerline at $y/D = 0$. Heat transfer is not considered in the study and adiabatic no-slip wall boundary conditions are used on the nozzle surface. Finally, the upstream boundary condition for the nozzle inlet specifies the total pressure and total temperature of the jet with an initial inlet $M = 0.15$ normal to the inlet plane. The inlet M may fluctuate and the total values of P and T are held constant. Full details of the computational grids and boundary conditions used in this simulation can be found in Miller et al. [10]. The numerical implementation and mathematical development are shown in Nelson and Power [16]. These boundary conditions are sufficient for a steady solution to be found when using an ideal gas. Some of the simulations use a helium–air mixture, and thus the mass concentration of the helium species is needed at the freestream and inlet boundary conditions. In the freestream the mass concentration of helium is zero and at the nozzle inlet the mass concentration is set to match the acoustic velocity at the nozzle exit as discussed earlier. When helium–air simulations are performed total temperature ratio (TTR) = 1.0 at the nozzle inlet.

Summary of Jet Operating Conditions

Experimental measurements are performed in the Pennsylvania State University jet noise facility with cold pure air and helium–air mixture jets. CFD simulations are performed using Wind-US for both heated jets and the corresponding helium–air mixtures. The jet conditions experimentally and numerically investigated are summarized in Table 1.

Two nozzles are used for the experimental measurements: a contoured, purely converging (design Mach number $M_d = 1.0$) nozzle and a converging-diverging nozzle designed with the method of characteristics to operate shock-free at a design Mach number $M_d = 1.5$. The coordinates of these nozzles are imported directly into the Gridgen software to create the computational domains for the corresponding Wind-US simulations.

Results

This section presents experimental and numerical results from the jet conditions summarized in Table 1. The streamwise velocities at two traverse locations, $x/D = 4$ and $x/D = 8$, for both the $M_j = 0.9$ and $M_j = 1.5$ jets at all temperature ratios are shown first, in Figs. 3 and 4. The numerical predictions at TTR = 1 are obtained with pure air, while the predictions of the TTR = 2.2 and TTR = 3.6 cases are obtained with both heated air and helium air mixtures. Experimental results are plotted as symbols, numerical results with heated air as solid lines, and numerical results with helium–air mixtures as dashed line. The first observation that can be made is that the numerical results from both methods collapse extremely well. This illustrates that there are little differences between the predicted velocity profile of a heated air jet and the corresponding helium–air jet. This demonstrates that the helium–air mixture provides velocity profiles that are similar to the corresponding heated jet condition. The experimentally determined velocity profiles also show good agreement with the numerical predictions. However, small discrepancies appear in the inner part of the mixing layer, where the experiments generally show lower velocity than the numerical results. CFD results of high-speed subsonic jets demonstrate lower mixing close to the nozzle exit relative to experimental data. In supersonic jets near $M_j = 1.5$, compressibility effects lower the mixing rate in the experiment, that in turn agree better with CFD results. These discrepancies are more visible in the nondimensionalized plots presented later. The centerline velocity obtained from both the CFD and the pitot measurements increases with increasing (simulated) TTR for a jet of given M. These velocities match the theoretical values presented in Table 1. In the region of the outer part of the jet, $r/D \geq 0.6$, the effects of helium (or heat) addition on the velocity profile is much less dramatic: the increase in velocity is very slight, and the curves quickly merge into one velocity profile. This is in agreement with measurements performed by Lau [2] with laser velocimetry in $M_j = 0.5$ heated jets of different temperature ratios.

It was also found by Lau et al. [17] that the nondimensionalized velocity profiles for isothermal jets show similarity if plotted as a function of the normalized radial distance $\eta = (r - r_{0.5})/x$, where $r_{0.5}$ is the radial location from the centerline that satisfies $U/U_j = 0.5$. The velocity magnitudes are normalized by the fully-expanded velocity. In this work the velocities are normalized by $\eta = (r - r_{0.5})/\delta_\omega$, where $\delta_\omega = U_{\max}/[\mathrm{d}U/\mathrm{d}r]_{\min}$ represents the vorticity thickness. In the work of Lau et al. [17] data was shown to follow a Görtler error function profile:

$$U_1/U_j = \frac{1}{2}[1 - \mathrm{erf}(\sigma\eta)] \tag{7}$$

Table 1 Jet operating conditions for the numerical simulations and experiments

M_d	M_j	$\mathrm{TTR}^{\mathrm{heated}}$	U_j, m/s	M_∞	T_j	χ_j^{He}, %	Φ_j^{He}, %	γ_j^{mix}	R_j^{mix}, $\mathrm{m^2\,K/s^2}$	a_j^{mix}, m/s
1.0	0.9	1.0	286	0.84	252	0	0	1.4	287	307
1.0	0.9	2.22	427	1.26	240	61.4	18.0	1.53	609	473
1.0	0.9	3.6	543	1.60	236	81.7	38.1	1.59	969	604
1.0	1.47	2.2	626	1.84	186	63.5	19.4	1.54	635	426
1.5	1.5	1.0	427	1.26	203	0	0	1.4	287	285
1.5	1.5	1.62	544	1.60	190	44.7	10.1	1.49	467	363
1.5	1.5	2.22	637	1.87	184	63.7	19.5	1.54	636	423
1.5	1.5	3.6	811	2.39	175	84.1	42.3	1.60	1044	542

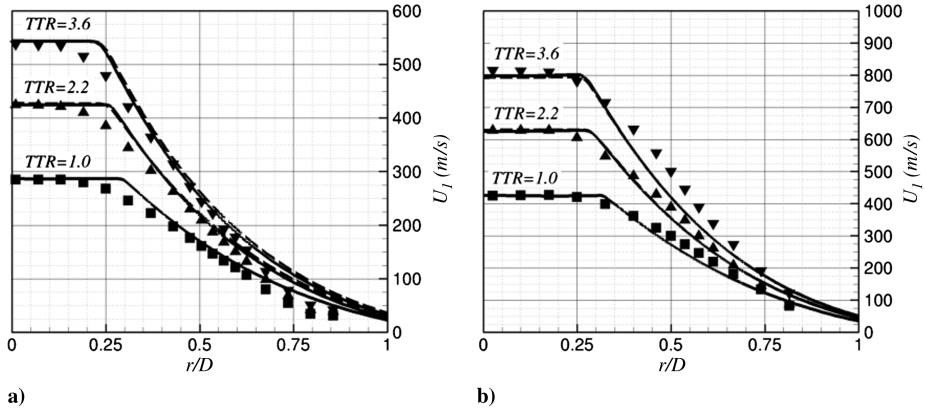

Fig. 3 Velocity profiles measured in jets of various TTR at $x/D = 4$. Heated simulations, helium–air simulations, and experiments are represented by solid lines, dashed lines, and symbols, respectively: a) $M_j = 0.90$ and b) $M_j = 1.50$.

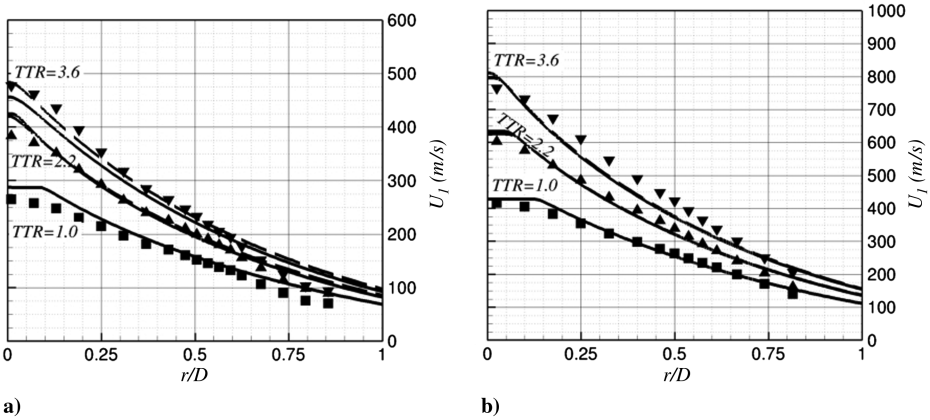

Fig. 4 Velocity profiles measured in jets of various TTR at $x/D = 8$. Heated simulations, helium–air simulations, and experiments are represented by solid lines, dashed lines, and symbols, respectively: a) $M_j = 0.90$ and b) $M_j = 1.50$.

where σ is found from a simple empirical formula $\sigma = 10.7/(1 - 0.273M_j^2)$, and erf is the error function. Similar measurements by Lau [2] showed the same collapse for heated jets. Equation (7) is not representative of a solution of the equations of motion and is not a model of the variation of the velocity in the shear layer, potential core, or far-field. It is an empirical fit to the measured or simulated velocity that is applicable at various streamwise locations of the jet. This includes the potential core region just downstream from the nozzle exit or the fully turbulent region. Performing a nondimensionalization of both the experimental data and numerical predictions of this study, shows that these velocity profiles are similar, as shown in Figs. 5 and 6. Both the CFD and the experimental results collapse across all temperature ranges and are therefore self-consistent. The helium–air simulation results also match very closely to the heated air results, providing confidence in the chemical frozen module of Wind-US. However, this representation highlights the discrepancies between the computational results and the experiments. The experimental results fit closely to an error function with coefficient $\sigma = 2.055$ for the $M_j = 0.9$ jets and $\sigma = 2.073$ for the $M_j = 1.5$ jets. On the other hand, the numerical results are overpredicting the velocity around $\eta = \pm 0.5$. This can be attributed to the limitation of the Menter SST model to correctly predict the spreading of the jet correctly, as previously discussed [10].

Because Wind-US has the ability to calculate the mass concentration of the helium species of the frozen chemistry model spatially, a direct comparison can be conducted with the experiments to further validate the assumptions made. The helium mass concentration values are plotted for both experimental and numerical data against the local velocity U_1 in Fig. 7 at streamwise locations $x/D = 4$ and $x/D = 8$. The experimental measurements are shown as scatter points and the computations are represented by lines. Clearly, each set of either numerical or experimental data shows an almost perfect linear relationship between the velocity and helium mass concentration. The experimental data were computed assuming such a relationship existed, following the analysis described in the Appendix. The fact that the numerical results follow

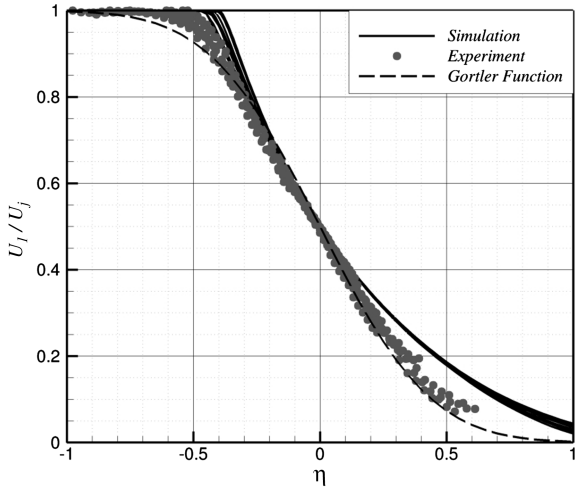

Fig. 5 Nondimensional radial mean velocity profiles measured in fully-expanded $M_j = 0.9$ jets at $x/D = 4$ and $x/D = 8$ of different simulated temperature ratios TTR = 1.0, TTR = 2.2, and TTR = 3.6. Heated and helium–air simulations are solid lines, dots are experimental measurements, and the dashed line is the Görtler function.

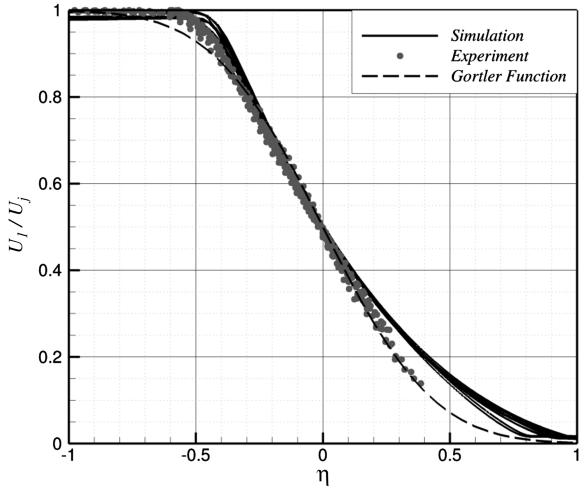

Fig. 6 Nondimensional radial mean velocity profiles measured in fully-expanded $M_j = 1.5$ jets at $x/D = 4$ and $x/D = 8$ of different simulated temperature ratios TTR = 1.0, TTR = 2.2, and TTR = 3.6. Heated and helium–air simulations are solid lines, dots are experimental measurements, and the dashed line is the Görtler function.

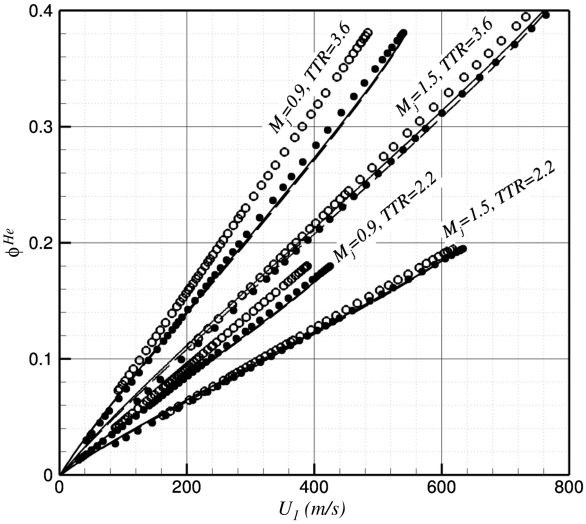

Fig. 7 Comparisons of the simulated and experimental helium mass concentration at $x/D = 4$ and $x/D = 8$ as a function of u m/s. Helium–air simulations and experiment are denotes by lines and circles, respectively. Data at $x/D = 4$ is represented by solid lines and solid circles and data at $x/D = 8$ is represented by dashed lines and hollow circles.

such a relationship also constitute a validation of the result of this analysis. It is difficult to distinguish between the experimental measurements obtained for different downstream locations of the same jet condition. This is not the case for the numerical results which show some discrepancies between different downstream locations. For the supersonic cases the slopes between the prediction and experiment match closer than with the subsonic case. At $x/D = 4$ the predictions match the experiments better relative to $x/D = 8$. This can be easily seen in the line plot for $M_j = 0.9$ and TTR = 3.6. The trend of the numerical data shows that as the downstream location is increased the helium concentration decreases with velocity relative to an upstream location. This is in contrast with the experimental data. This implies that the turbulent mixing of the simulations is not as efficient as it should be as the experiments show. The predicted potential core length does not match the experiment, and is very typical of modern large eddy simulations and steady RANS simulations, due to the underprediction of the spreading rate discussed earlier. As a result, this larger centerline velocity creates the slight discrepancy in the slopes observed in Fig. 7. This discrepancy is therefore not due to the helium–air frozen chemistry model, which is still believed to perform adequately.

The helium concentration can also be plotted as a function of the radial position, as shown in Fig. 8 for the experimental conditions of Table 1 and the corresponding helium–air mixture simulations. The values of the helium concentration are shown at the two downstream measurement locations of $x/D = 4$ and 8. The agreement on the centerline, $r/D = 0$, is very good. This is not the case in the shear layer region of the heat-simulated cases. This illustrates that the known quantities at the inlet boundary condition of the nozzle are specified correctly relative to the known helium concentration in the plenum of the experimental facility. Outside of the jet in the entrainment region, the simulations also have captured the experimental data closely. In the shear layer region the numerical results are less satisfactory relative to the experimental measurements. This is especially true as the helium concentration increases. For example for TTR = 3.6 and $M_j = 1.5$, at $r/D = 0.5$ the simulations under predict the helium concentration by up to 25% compared with the experiment and by 22% at $x/D = 8$. As mentioned before, the turbulence model does not correctly capture the jet spreading rate, resulting in some discrepancies very similar to the ones observed in Figs. 3 and 4. These discrepancies are not due to the additional use of the frozen chemistry model for helium–air mixtures. The steepened mean-flow profiles of the predictions relative to the experimental results has an effect on the helium mass concentration.

Cross-stream temperature profiles of the $M_j = 0.9$ jets can be seen in Fig. 9. The solid lines correspond to the static temperature, as obtained from heated air numerical simulations. The experimental points correspond to the static temperature as simulated by the local helium concentration. Similar to the profiles of U_1, the spatial variables have been normalized by the nozzle diameter D.

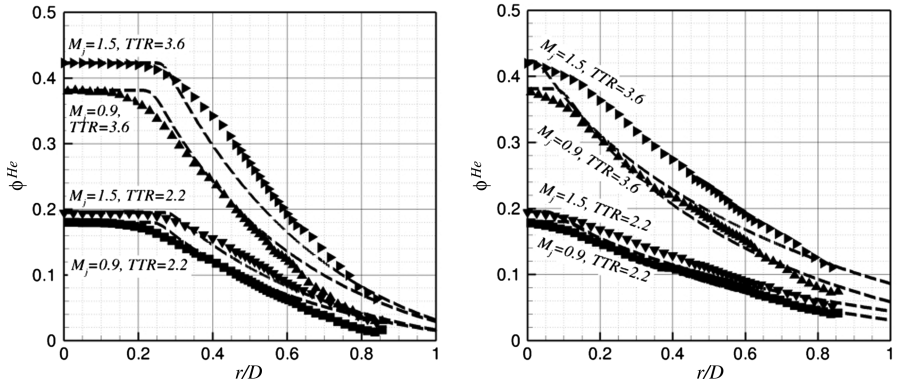

Fig. 8 Comparisons of the simulated and experimental helium mass concentration as a function of r/D: a) $x/D = 4$ and b) $x/D = 8$. Helium–air simulations and experiments are represented by dashed lines and symbols, respectively.

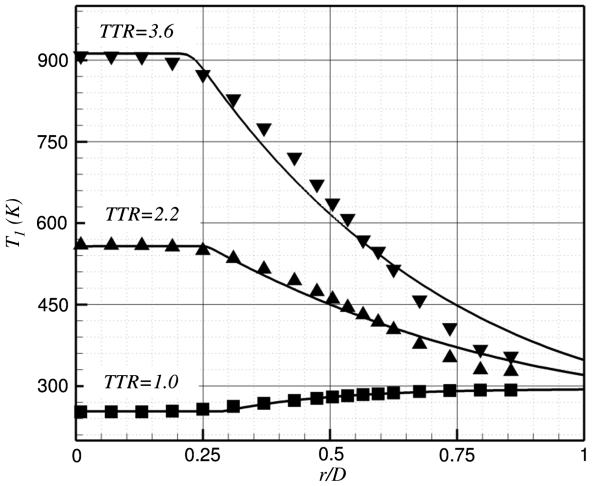

Fig. 9 Temperature profiles measured in the $M_j = 0.9$ jets at $x/D = 4$. Heated simulations and experiments are represented by solid lines and symbols, respectively.

Dimensional units of Kelvin have not been normalized in order to illustrate the differences in simulated temperatures of the various $M_j = 0.9$ jets. Only the cross-stream profiles at $x/D = 4$ are shown. The agreement is excellent at TTR = 1 but less satisfactory at TTR = 3.6. The centerline temperatures from the simulation, like those in Fig. 8 correspond to the experimental measurements. The shear layer simulated values of temperature for the heated jets diverge from the experiment for the heated cases by a small amount. For the TTR = 3.6 case and at $r/D = 0.75$ the values diverge by as much as 16%. For the TTR = 2.2 case the results diverge by as little as 5%. Since the simulations are performed for a heated air jet and corresponding simulated quantities are not calculated from the helium–air concentration, this constitutes a very good validation of the processing approach used for the experimental data as well as the ability to properly simulate heat with the addition of helium.

Since the local speed of sound is calculated at each radial location of the experimental data, local Mach number (M_1) profiles can be compared with corresponding numerical simulations, as shown in Fig. 10. Figure 10 shows the radial distribution of M_1 at $x/D = 4$ in part (a) and $x/D = 8$ in part (b). Both the simulated heated air and helium–air mixture results are also shown. On the nozzle lip line the predictions match experiment. The simulations show a much larger entrainment of the flow than the experiment as shown near $r/D = 0.8$ at both streamwise locations. Potential core length of the simulation is also much longer than the experiment causing values of M_1 to be artificially higher at $x/D = 8$. Trends of simulated M_1 where the potential core meets the shear layer are also incorrect and do not fall off in a smooth fashion as the Görtler function or the experimental data. Heated simulations agree better with experimental data for M_1. This observation is in contrast to helium concentration comparisons as shown in Fig. 8, where the heated simulations compare less favorably relative to moderate or no heating.

Schlieren images of the $M_j = 1.5$ jet operating on- and off-design are obtained using helium–air mixtures to simulate the various TTR. Corresponding images from numerical prediction can be constructed by post processing the density flowfield. The process of constructing numerical schlieren from steady RANS data is described in Miller et al. [10]. A comparison of the supersonic $M_d = 1.0$, $M_j = 1.5$, TTR = 2.2 jet is shown in Fig. 11a. The top image in a) is produced experimentally with a *Z*-type schlieren setup described in Veltin and McLaughlin [18]. The images presented result from a large number of spark schlieren images averaged in order to obtain a better visualization of the shock-cell structure and spreading angle. As a side effect, small-scale structures are less apparent. Averaging is not required to produce numerical schlieren. The middle and bottom image of part (a) is representative of the numerical schlieren. The middle numerical schlieren uses heated air and the bottom image shows the helium–air jet for a simulated TTR = 2.2. Qualitative comparisons can be made by examining the images. In general the on-design case shows good overall agreement with the experiment. The shock-cell structure may be faintly seen in the experimental schlieren but are much more apparent in the numerical simulation. Wind-US inherently assumes that the boundary layer is turbulent and never laminar and no-tripping of the boundary layer occurred in the nozzle interior. This is obviously not representative of the physics of these small jets with Reynolds number around 400,000 that possibly possess laminar boundary layers within the entire nozzle length. Since turbulent boundary layers have a different displacement thickness than laminar ones, the simulation produces slight shocks when operating at $M_j = 1.5$. The convergent-divergent nozzle used in the experiment is designed to operate with a fully-expanded jet and a laminar boundary layer at $M_d = 1.5$. The shock-cell length also exhibits a slight change when operating with a helium–air mixture. Both jets are very close to M_j but are slightly different due to very small variations in the flow properties (such as a slightly decreased viscosity due to a different gas species in the nozzle). The off-design parameter of the shock-cell structure is extremely small.

A second schlieren comparison is made in Fig. 11b and illustrates the heated off-design case of $M_d = 1.0$, $M_j = 1.47$, and TTR = 2.2. The arrangement of the images are the same as in part (a). This case uses the convergent nozzle in both the schlieren experiment and simulations. The same method to produce the numerical schlieren of Fig. 11a is also used here with the same continuous contours and range. Excellent qualitative agreement may be observed with regard to the shock-cell structure position between the predictions and experimental results. Positions of these shocks are controlled mainly

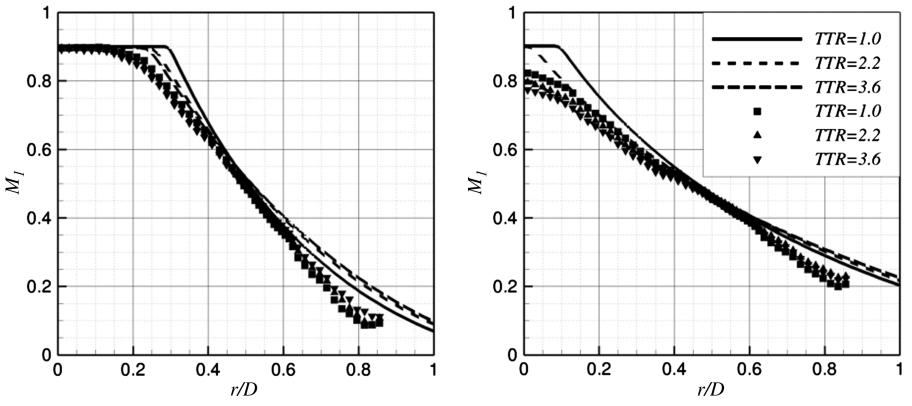

a) b)

Fig. 10 Mach number profiles of the numerical and experimental data for the $M = 0.90$ jet operating at various temperature ratios: a) radial location $x/D = 4$ and b) radial location $x/D = 8$. Heated simulations, helium–air simulations, and experiments are represented by solid lines, dashed lines, and symbols, respectively.

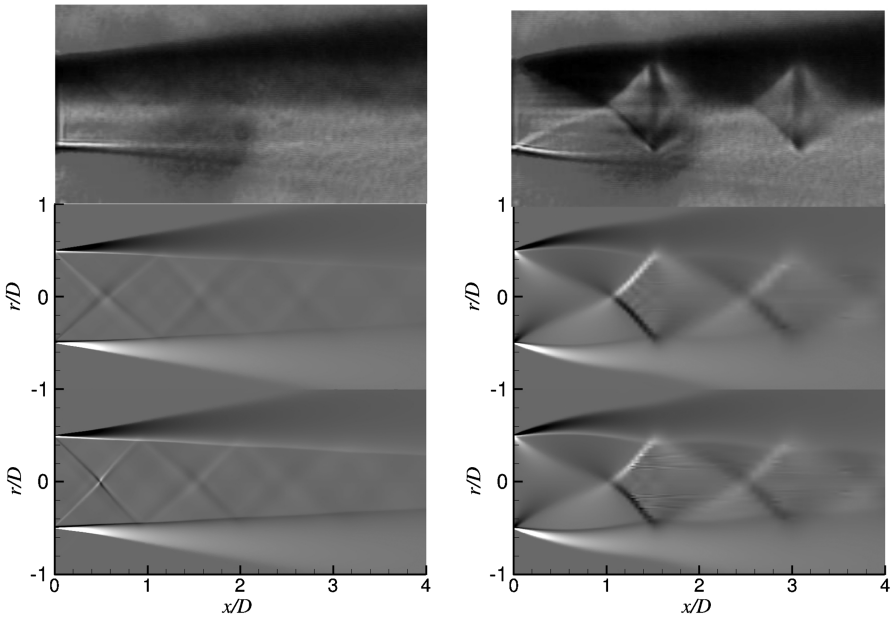

a) M_d = 1.50, M_j = 1.50, *TTR* = 2.20 jet b) M_d = 1.00, M_j = 1.50, *TTR* = 2.20 jet

Fig. 11 Comparisons of *Z*-type schlieren with numerically generated schlieren. The top images are produced by the *Z*-type experimental schlieren and the middle and bottom are numerically generated results produced by heated air or helium–air mixtures, respectively.

by the inviscid terms of the model equations and boundaries by the termination of the potential core in the cross-stream directions. Though, from examinations of the simulations it is known that there is more entrainment than in the experiment, as this phenomena is controlled more so by viscous effects.

Mach number contour plots are created from the numerical results of the $M_d = 1.0$, $M_j = 0.9$, and TTR $= 2.20$ and $M_d = 1.5$, $M_j = 1.5$, and TTR $= 3.6$ jets. These are illustrated in Fig. 12. In part (a) and (b) the top half plane is representative of a simulated heated air result and the bottom half plane is the helium–air result. For the $M_j = 0.9$ jet the qualitative agreement between the two is excellent. The core lengths and shear layer growth of both the heated air and helium–air mixture are almost the same. The same agreement of core length and shear layer growth may also be seen in the supersonic case of part (b), however, there is some slight discrepancy between the shock-cell structures similar to the observation made from the schlieren images. These once again, can be attributed to thicker boundary layers and changes in γ due to helium in contrast to air. It is

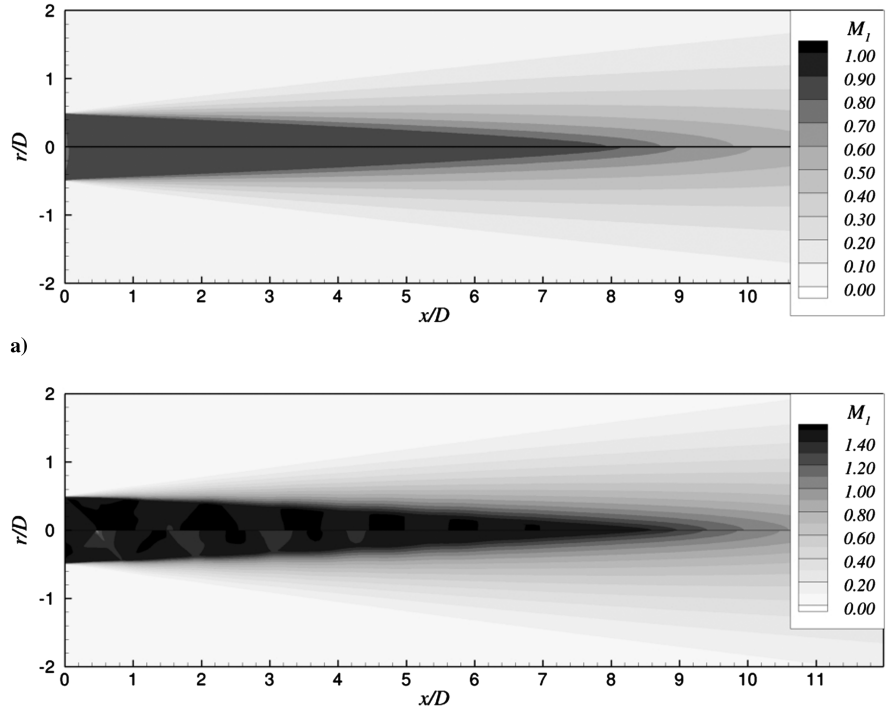

a)

b)

Fig. 12 Contour plots of *M* for the a) $M_d = 1.0$, $M_j = 0.90$, TTR $= 2.20$ and b) $M_d = 1.50$, $M_j = 1.50$, TTR $= 3.60$ jets. The top half planes, $y > 0$ are contours of the heated simulated air jet while the bottom half planes, $y < 0$ are representative of contours of the helium–air jet.

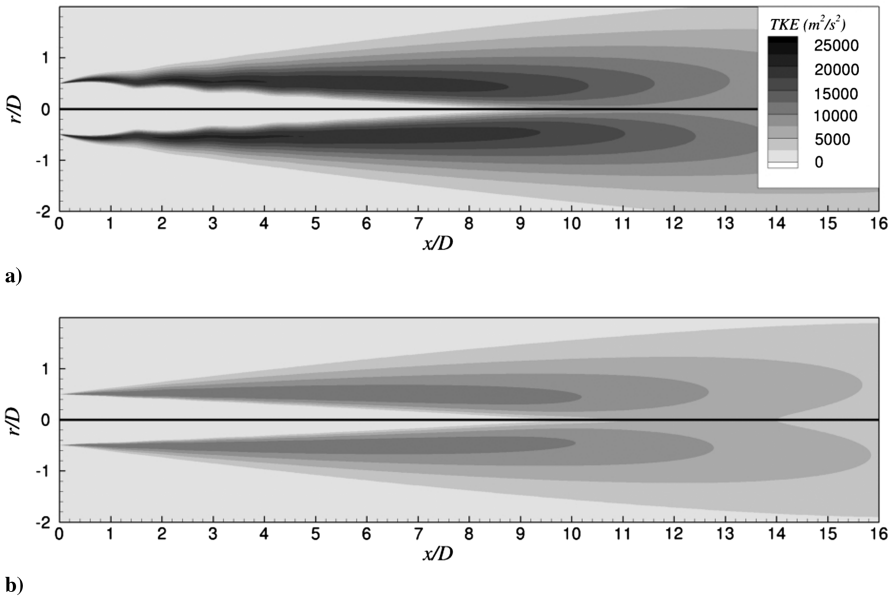

Fig. 13 Contour plots of the TKE. The top half planes show the heated air results and the bottom half planes show the helium–air simulated results: a) $M_d = 1.00$, $M_j = 1.50$, and TTR = 3.60 jet and b) $M_d = 1.50$, $M_j = 1.50$, and TTR = 2.20 jet.

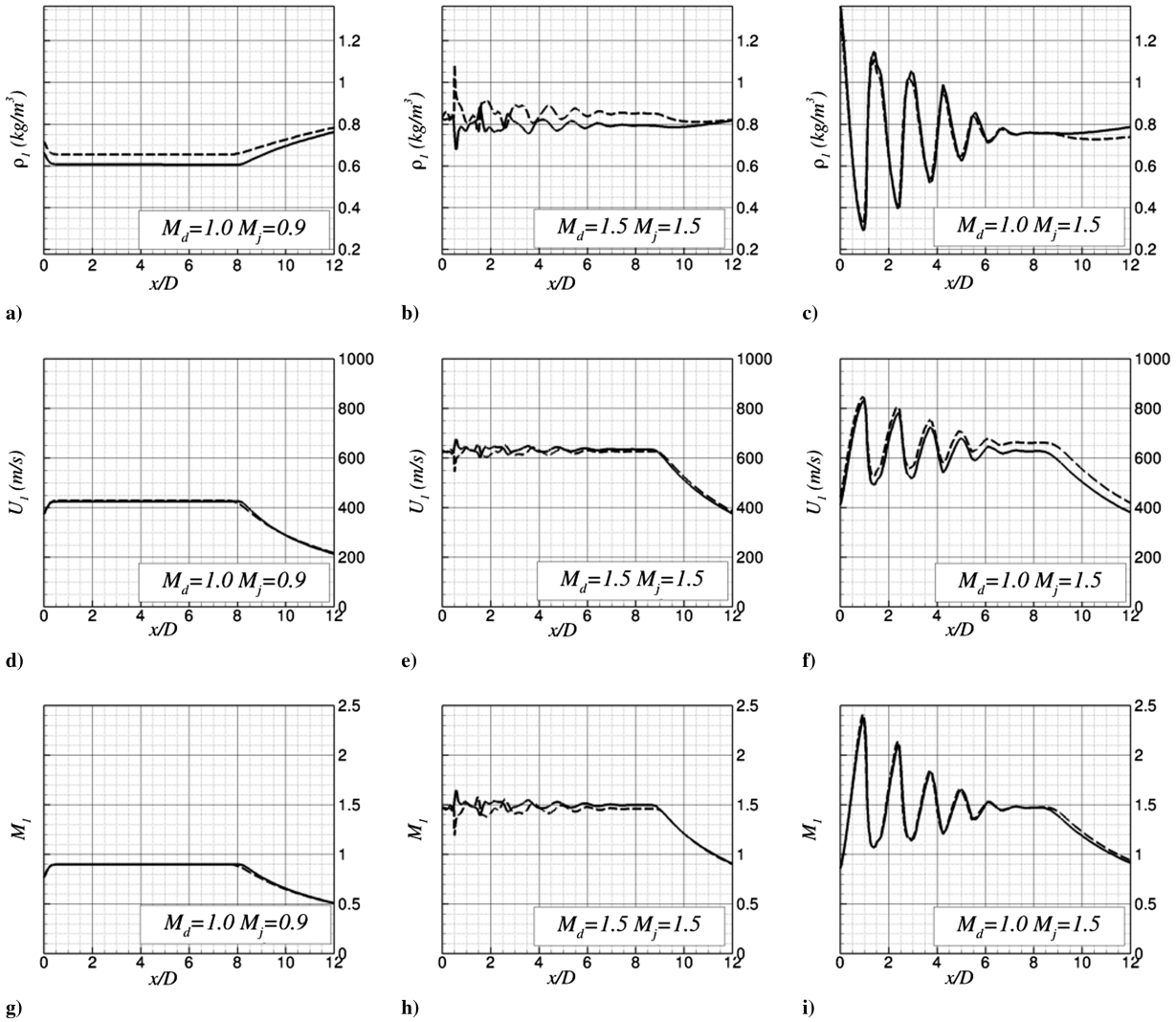

Fig. 14 Various centerline comparisons of TTR = 2.2 jets: —— air; — — helium–air.

encouraging that the simulations of heated air and helium–air jets agree, however, the differences between the predictions and experiments remains as shown in the previous discussions.

Jet mixing and broadband shock-associated noise is closely tied to the turbulence levels in jets. Therefore, it is constructive to examine the differences of the turbulent kinetic energy (TKE) between heated air and helium–air jets that simulate the same heated condition. Figure 13 shows contour plots of TKE. The upper half planes are contours of TKE of heated air simulations and the bottom half planes are contours of TKE of helium–air simulations. Part (a) of the figure is the $M_d = 1.00$, $M_j = 1.50$, and TTR $= 3.60$ jet and part (b) is the $M_d = 1.50$, $M_j = 1.50$, and TTR $= 2.20$ jet. The off-design jet clearly has its TKE field effected by the shock-cell structure while the jet operating on-design spreads smoothly due to an almost shockless jet plume. Interestingly, the TKE is slightly higher and extends further downstream in the helium–air off-design simulation than the equivalent hot jet. This is in contrast to the on-design case where the TKE is in much better agreement. The presence of shocks, which are partially a function of γ, effect the TKE contour fields between heated and helium–air jets. Though this effect is relatively small as seen by looking at the contour levels of TKE. The levels of TKE in part (a) far downstream can differ in the streamwise direction by up to a jet diameter while in part (b) differ by as much as a tenth of a jet diameter. There is no shock capturing scheme present in Wind-US at the time of the publication of this paper, which could potentially vastly improve these results.

Centerline plots are produced for ρ_1, U_1, and M_1 from simulations of $M_j = 0.9$ and $M_j = 1.5$ heated and heat-simulated jets at TTR $=$ 2.2 and TTR $= 3.6$ in Figs. 14 and 15 respectively. In both figures the rows of subfigures are representative of ρ_1, U_1, and M_1 while the columns correspond to the different operating conditions. Since the helium–air concentrations are chosen to match the exit acoustic Mach number M_∞ for both TTR values, the values of M_1 at the exit of the nozzle ($x/D = 0$) matches perfectly between the mixture and the heated air simulations. For example, in part (g) of Fig. 14 M_1 is almost identical along the centerline axis. The same excellent agreement can be seen in other cases also. Only for the supersonic cases does the core extend slightly farther with the helium–air jets compared with the heated air jets. As expected, comparisons of the density for both temperature ratios and three corresponding jet conditions do not exhibit the same level of agreement. This is due to the fact previously stated that it is not possible to match both the density and the Mach number. While these simulations are performed by matching M_∞ between heated air and helium–air jets, the calculation could easily have been performed by matching the exit densities. The values of the streamwise velocity, U_1, on the centerline agree very favorably for the subsonic case, as seen in Figs. 14 and 15 for both TTR and M_j values. These plots in particular illustrate the slightly longer core lengths of the helium–air simulations.

The centerline values of the supersonic on-design jet ($M_d = M_j = 1.5$) with heated air and helium–air demonstrate that the core lengths are nearly the same. Also, it can be seen in part (h) of both figures that the values of M_1 at the jet exit have a very small difference. The pattern of fluctuations in the centerline Mach number for the supersonic on-design jet suggests that the helium–air jet is

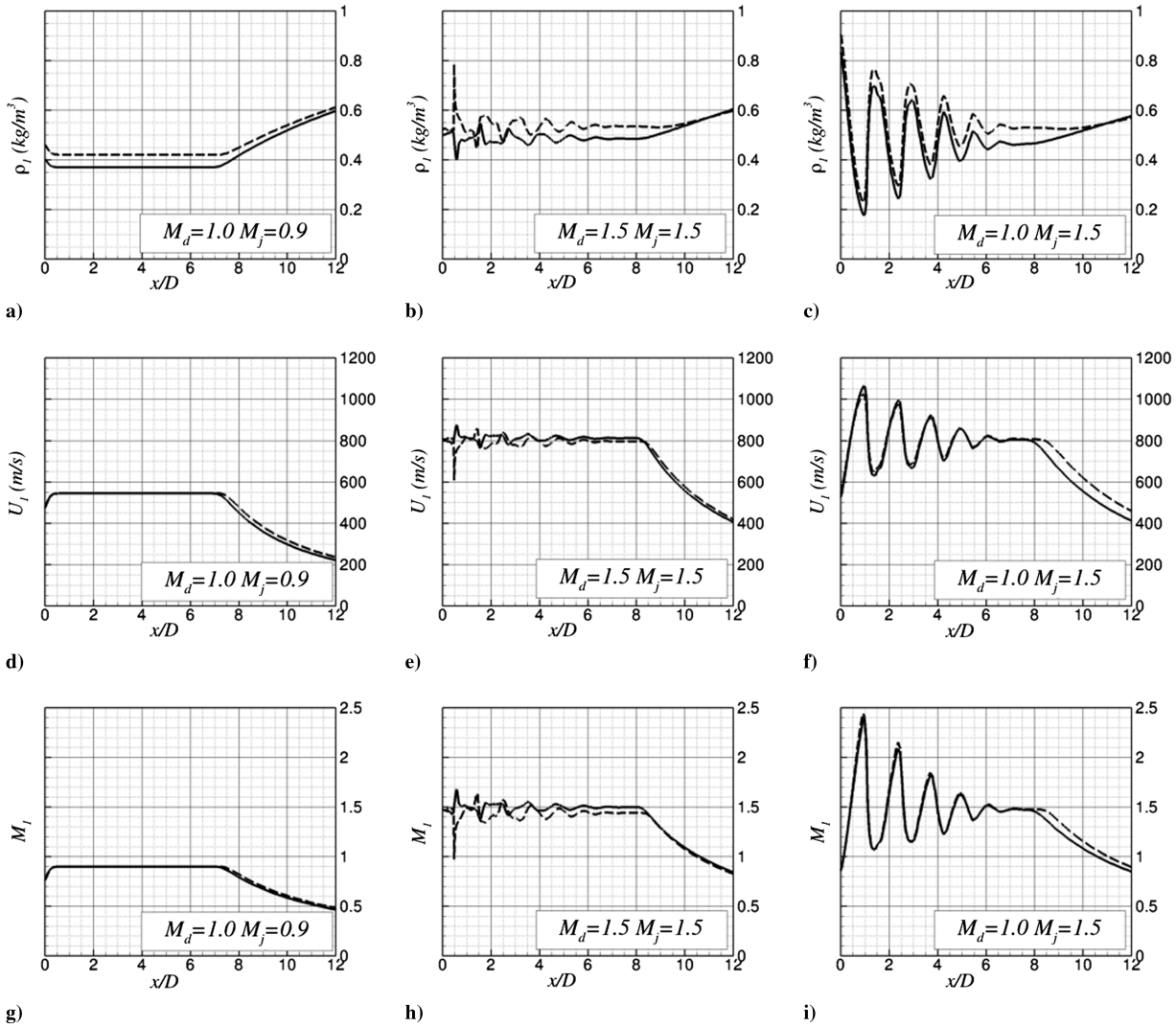

Fig. 15 Various centerline comparisons of TTR = 3.6 jets: —— air; — — helium–air.

slightly overexpanded while the heated air simulated jet is underexpanded. Indeed, the rise or fall of velocity due to shocks or Prandtl–Meyer expansion waves can be seen in the centerline plots. These values of M_j at the jet exit are extremely close to the design Mach number $M_d = 1.5$. Their slight difference produces shock cells of different lengths, as already observed from the schlieren images and the Mach number contour plots. When examining the discontinuities of M_1 in part (h) of both Figs. 14 and 15, it appears that there is an initial very strong shock. However, this is an artifact of using the axisymmetric boundary condition where $\partial P_1/\partial r = 0$. This condition is theoretically true at a point; however, it is enforced in CFD by using grid points that are on the centerline axis and the corresponding grid points of the spatial discretization stencil in the cross-stream direction. Therefore, there is a numerical effect of broadening the region where $\partial P_1/\partial r = 0$. This effect can be varied by changing the grid spacing in the cross-stream direction near the centerline, effectively causing a barrel shock that has the diameter on the order of twice the distance from the centerline to the first grid point in the cross-stream direction. To minimize this effect, the grid point clustering in the cross-stream direction on the centerline axis uses the same distribution as the nozzle wall at $x/D = 0$.

Conclusions

Experimental and numerical comparisons of the flow properties of high-speed helium–air mixture and heated air jets demonstrate overall good agreement. There are some discrepancies between the simulations and experiments that are mainly attributed to the lack of good turbulence models for heated jet flows. Flowfields of helium–air jets show properties that are very similar to heated air jet measurements present in the literature. In particular, the TKE in both cases is almost identical according to steady RANS predictions, and are validated with corresponding experiments. An important result that is shown is that the species concentration of helium varies linearly in the cross-stream direction of the jet. Cross-stream comparisons of helium–air concentrations from steady RANS calculations and experiment show good agreement, especially for moderately heated jets. The Menter SST turbulence model used in the simulation is observed to underpredict the growth rate of the jet for the lower jet Mach number cases, leading to a misprediction of the potential core length. However, the very good agreement between simulated heated air and helium–air mixture jets provide a validation of the frozen chemistry model used, as well as further evidence that the helium addition does indeed provide mean flow properties similar to heated air. Turbulent kinetic energy comparisons between the simulations for on-design jets shows little variation. Some differences are seen between the TKE for off-design supersonic jets, but this is probably due to a lack of a shock capturing scheme. Most importantly, the validation of the flowfield properties of high-speed helum-air jets provides confidence regarding the use of small-scale anechoic facilities for heated jet noise research.

Appendix: Helium Mass Concentration in Helium–Air Jets

In steady axisymmetric turbulent jets the conservation of momentum in the x (streamwise) direction can be expressed as follows:

$$\rho u \frac{\partial u}{\partial x} + \rho v \frac{\partial u}{\partial r} - \frac{\partial}{\partial r}\left(\mu_t \frac{\partial u}{\partial r}\right) = -\frac{\partial P}{\partial x} \tag{A1}$$

where μ_t represents the eddy viscosity, or the effective viscosity of a turbulent fluid, and u and v are, respectively, the axial and radial components of the velocity. Note that the normal stress contribution is neglected. In subsonic jets and supersonic jets operating on-design the static pressure at the nozzle exit is equal to the ambient pressure. Thus the streamwise gradient of pressure can be neglected ($\partial P/\partial x$), such that the right hand side term is dropped. Then, within the jet mixing layer, three different phenomena can cause mixing of the jet inner gas mixture with the ambient air: turbulent mixing, molecular diffusion, and thermal diffusivity. Turbulent mixing can be described, as shown by Spalding [19], using the conservation of mass of the entrained flow. The resulting equation relates the mass concentration of helium Φ^{He} to the spatial velocity field:

$$\rho u \frac{\partial \Phi^{\mathrm{He}}}{\partial x} + \rho v \frac{\partial \Phi^{\mathrm{He}}}{\partial r} = \frac{\partial}{\partial r}\left(\frac{\mu_t}{Sc_t}\frac{\partial \Phi^{\mathrm{He}}}{\partial r}\right) \tag{A2}$$

where Sc_t refers to the turbulence Schmidt number. When mixing occurs via molecular and thermal diffusion (of helium), rather than turbulent mixing, then the following equation, based on Fick's law and derived by Schlichting and Gersten [15] is used:

$$\rho u \frac{\partial \Phi^{\mathrm{He}}}{\partial x} + \rho v \frac{\partial \Phi^{\mathrm{He}}}{\partial r} = \frac{\partial}{\partial r}\left[\rho D_{12}\left(\frac{\partial \Phi^{\mathrm{He}}}{\partial r} + k_T \frac{\partial(\ell_n T)}{\partial r}\right)\right] \tag{A3}$$

where D_{12} denotes the coefficient of binary diffusion of helium in air and k_T the thermal diffusion ratio. However, even though the jets of interest are not isothermal, they are unheated and therefore do not have large enough temperature gradients to produce appreciable thermal diffusion relative to other mechanisms. The thermal diffusion term can therefore be neglected. The remaining molecular diffusivity term is compared with the right hand side term of Eq. (A2). The coefficient of molecular diffusion of helium in air is a known quantity, with value $D_{12} \simeq 62.10^{-6}$ m^2/s at ambient conditions. Therefore, the term ρD_{12} is of the order of magnitude 10^{-4}. Also, the turbulent kinematic viscosity ν_t can be estimated, as shown by Schlichting and Gersten [15] and by Spalding [19] as $\nu_t = 0.026 \times r_{0.5} \times U_c$, where $r_{0.5}$ is the half velocity point and U_c is the centerline velocity of the jet. This leads to a dynamic viscosity μ_t with an order of magnitude 10^{-1} for the jets considered ($D = 0.0127$ m and $U_j = 300$ to 600 m/s). Using an estimated value of 0.7 for the turbulent Schmidt number, Sc_t, as suggested by Panchapakesan and Lumley [20], the constant in the right hand side of Eq. (A2) has an order of magnitude of 10^{-1}. This is much higher than the order of magnitude 10^{-4} obtained for the molecular diffusion. Therefore, molecular diffusion is neglected, which leaves turbulent mixing as the dominant mechanism by which helium is radially transported in the jet shear layer and plume. Equations (A1) and (A2) are therefore the only equations to consider. Previous studies [20,21] have shown that while the value of Sc_t varies across the shear layer, a constant value of 0.7 can be used and produces adequate concentration estimates. Therefore, Sc_t is assumed constant and moved outside the partial derivatives. It was also shown by Spalding [19] that the turbulence viscosity μ_t is quasi constant until the half velocity point and decreases slowly further outward. Therefore, the derivative of μ_t with respect to radial displacement can be neglected, especially compared with the large velocity gradient through the mixing layer. μ_t is therefore moved outside of the partial derivatives. Furthermore, assuming the mass concentration of helium can be expressed as a sole function of the local flow velocity U_1, the chain rule for partial derivative can be applied to Eq. (A2), and then combined with Eq. (A1). These mathematical operations yield

$$\left(\frac{1}{Sc_t} - 1\right)\frac{\partial \Phi^{\mathrm{He}}}{\partial U_1}\frac{\partial^2 U_1}{\partial r^2} + \frac{1}{Sc_t}\frac{\partial^2 \Phi^{\mathrm{He}}}{\partial U_1^2}\left(\frac{\partial U_1}{\partial r}\right)^2 = 0 \tag{A4}$$

To obtain a solution for this second order differential equation the function $U_1(r)$ must be known. It was observed in past experimental studies [17] that the velocity profile in a jet follows a Görtler error function distribution, with amplitude proportional to the jet velocity U_j. The first and second derivative of such a function is also proportional to U_j. As a result, the second term of Eq. (A4) is proportional to the square of the mean velocity, which means the first term can be neglected. Equation (A4) then reduces to a simple linear variation of the mass concentration of helium with respect to velocity. Following this development, reduction of the pressure data is performed with the underlying assumption that the helium concentration varies linearly with local velocity. Numerical and experimental results shown in this paper show the validity of this argument.

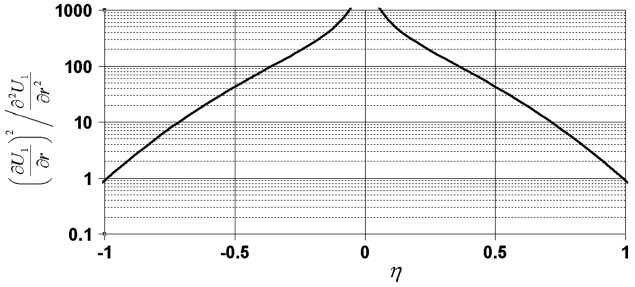

Fig. A1 Ratio of the square of the radial derivative of the velocity with its second derivative, as a function of η.

As seen in the result part of the body of the manuscript, the velocity data obtained from experiment can be modeled by an error function. Therefore, the first and second derivative of the velocity profile with respect to radial distance can easily be computed. In the previous section, Eq. (A4) is solved by making the assumption that the second derivative of the velocity profile is negligible compared with the square of its first derivative. The two quantities can be compared by plotting their ratio, as shown in Fig. A1. It is obvious from this plot that for any value η comprised between -0.7 and 0.7 the ratio mentioned preceding is greater than 10. Since this η range corresponds to the whole mixing layer, this demonstrates that the first term of Eq. (A4) can indeed be neglected, leading to a helium concentration that varies linearly with the streamwise velocity.

It is noteworthy to mention that the same result can be obtained by making the assumption that the Schmidt number is unity throughout the mixing layer. However, since evidence [20,21] exist for the Schmidt number to have a different value (0.7), making such an assumption raises question as to the validity of the results. The approach described tries to rely on assumptions that are justify by experimental evidence so as to gain more faith in the validity of the results.

Acknowledgments

The experiments were partially supported through the NASA Research Announcement Cooperative Agreement NNX07AC88A. The Technical Monitor for the Cooperative Agreement is Milo Dahl of the NASA Glenn Research Center. The authors would like to express their gratitude to Philip Morris and Dennis McLaughlin for their consultation as well as Nick Georgiadis of the NASA Glenn Research Center for helpful discussions regarding the Wind-US code. Joo Kyung Suh of Raytheon Missile Systems is acknowledged for assembling the chemistry coefficient file.

References

[1] Tanna, H. K., Dean, P. D., and Fisher, M. J., "The Influence of Temperature on Shock-Free Supersonic Jet Noise," *Journal of Sound and Vibration*, Vol. 39, No. 4, 1975, pp. 429–460. doi:10.1016/S0022-460X(75)80026-5

[2] Lau, J., "Effects of Exit Mach Number and Temperature on Mean-Flow and Turbulence Characteristics in Round Jets," *Journal of Fluid Mechanics*, Vol. 105, 1981, pp. 193–218. doi:10.1017/S0022112081003170

[3] Seiner, J. M., Ponton, M. K., Jansen, B. J., and Lagen, N. T., "The Effects of Temperature on Supersonic Jet Noise Emission," German Society for Aeronautics and Astronautics/AIAA Paper 92-02-046, 1992.

[4] Tam, C. K. W., and Chen, P., "Turbulent Mixing Noise from Supersonic Jets," *AIAA Journal*, Vol. 32, No. 9, 1994, pp. 1774–1780. doi:10.2514/3.12173

[5] Doty, M. J., and McLaughlin, D. K., "Acoustic and Mean Flow Measurements of High Speed Helium Air Mixture Jets," *International Journal of Aeroacoustics*, Vol. 2, No. 3, 2003, pp. 293–334. doi:10.1260/147547203322986151

[6] Kinzie, K., and McLaughlin, D. K., "Measurement of Supersonic Helium–Air Mixture Jets," *AIAA Journal*, Vol. 37, No. 11, 1999, pp. 1363–1369. doi:10.2514/2.634

[7] Papamoschou, D., "Acoustic Simulation of Coaxial Hot Air Jets Using Cold Helium–Air Mixture Jets," *Journal of Propulsion and Power*, Vol. 23, No. 2, March–April 2007, pp. 375–381. doi:10.2514/1.21776

[8] Bridges, J., and Brown, C. A., "Validation of the Small Hot Jet Acoustic Rig for Aeroacoustic Research," AIAA Paper 2005-2846, 2005.

[9] Kuo, C.-W., Veltin, J., and McLaughlin, D. K., "Acoustic Measurements of Models of Military Style Supersonic Nozzle Jets," AIAA Paper 2009-18, 2009.

[10] Miller, S. A. E., Veltin, J., Morris, P. J., and McLaughlin, D. K., "Assessment of Computational Fluid Dynamics for Supersonic Shock Containing Jets," *AIAA Journal*, Vol. 47, No. 11, 2009, pp. 2738–2746. doi:10.2514/1.44336

[11] Menter, F. R., "Two-Equation Eddy-Viscosity Turbulence Models for Engineering Applications," *AIAA Journal*, Vol. 32, No. 8, Aug. 1994, pp. 1598–1605. doi:10.2514/3.12149

[12] Yoder, D. A., Georgiadis, N. J., and O'Gara, M. R., "Frozen Chemistry Effects on Nozzle Performance Simulations," AIAA Paper 2008-3909, 38th Fluid Dynamics Conference and Exhibit, Seattle, WA, 23–26 June 2008.

[13] Towne, C., "Wind-US User's Guide," http://www.grc.nasa.gov/www/winddocs/user/user.pdf [retrieved 22 May 2009].

[14] McBride, B. J., Gordon, S., and Reno, M. A., "Thermodynamics Data for Fifty Reference Elements," NASA TM-3287, Jan. 1993.

[15] Schlichting, H., and Gersten, K., *Boundary Layer Theory*, Springer, New York, 2003.

[16] Nelson, C., and Power, G., "The NPARC Alliance Flow Simulation System," AIAA Paper 2001-0594, Jan. 2001.

[17] Lau, J., Morris, P. J., and Fisher, M. J., "Measurements in Subsonic and Supersonic Free Jets Using a Laser Velocimeter," *Journal of Fluid Mechanics*, Vol. 93, 1979, pp. 1–27, 193–218. doi:10.1017/S0022112079001750

[18] Veltin, J., and McLaughlin, D. K., "Noise Mechanisms Investigation in Shock Containing Screeching Jets Using Optical Deflectometry," AIAA Paper 2008-2889, 14th AIAA/CEAS Aeroacoustics Conference, Vancouver, May 2008.

[19] Spalding, D. B., "Concentration Fluctuations in a Round Turbulent Free Jet," *Chemical Engineering Science*, Vol. 26, No. 1, 1971, pp. 95–107. doi:10.1016/0009-2509(71)86083-9

[20] Panchapakesan, N. R., and Lumley, J. L., "Turbulence Measurements in Axisymmetric Jets of Air and Helium. Part 2. Helium Jet," *Journal of Fluid Mechanics*, Vol. 246, 1993, pp. 225–247. doi:10.1017/S0022112093000102

[21] Yimer, I., Campbell, I., and Jiang, L.-Y., "Estimation of the Turbulent Schmidt Number from Experimental Profiles of Axial Velocity and Concentration for High-Reynolds-Number Jet Flows," *Canadian Aeronautics and Space Journal*, Vol. 48, No. 3, 2002, pp. 195–200.

C. Bailly
Associate Editor